J. Min. Metall. Sect. B-Metall. 61 (2) (2025) 235 - 250

Journal of Mining and Metallurgy, Section B: Metallurgy

EFFECT OF REDUCTION RATIO ON DIE FILL-OUT AND HARDNESS PROFILE OF COLD-DRAWN POLYGONAL RODS MADE OF ACID RESISTANT STEEL X6CrNiTi18-10

M. Rumiński [a], P. Skubisz [a,*], P. Micek [b]

[a] AGH University of Krakow, Faculty of Metals Engineering and Industrial Computer Science, Krakow, Poland

[b] AGH University of Krakow, Faculty of Mechanical Engineering and Robotics, Krakow, Poland

(Received 17 July 2025; Accepted 06 October 2025)

Abstract

The study investigates the effect of the reduction ratio on strain hardening efficiency and load during the drawing process of austenitic acid-resistant steel X6CrNiTi18-10. The focus is on optimizing geometry-related process conditions to achieve the highest quality and productivity when drawing special-purpose rods with polygonal shapes, specifically square and hexagonal cross-sections. The research addresses how increasing the reduction ratio can enhance strain hardening while reducing the number of drawing passes, ultimately affecting quality and load. Numerical modeling was used to analyze the relationship between strain hardening and load versus the reduction ratio. Proper models and assumptions were formulated and subsequently verified through experiments, which confirmed the validity of the mathematical and numerical models for load estimation. The study quantified the effect of strain on strength properties by mapping of measured hardness along the strain gradient. The application of variable billet diameters produced a similar hardness profiles for both analyzed rod geometries and reversed the effect on underfilling of the corners. The findings indicate a threshold reduction ratio for producing sound rods with square or hexagonal cross-sections. Exceeding this threshold can cause excessive strain hardening, leading to increased hardness that impedes corner fill-out and/or results in failure.

Keywords: *Cold drawing; Acid resistant steel; X6CrNiTi18-10 steel; Strain hardening; Finite element modeling; Hardness*

1. Introduction

Austenitic stainless steels find their application in numerous fields where resistance to corrosion in combination with decent strength is required [1]. The special operational characteristics make them unmatched engineering materials in many fields, mostly in automotive, construction, chemical, food, aircraft, energy, power and machine-building industries [2, 3]. Long products (rods, bars, wires and profiles) made of stainless steels which must exhibit good surface and dimensional quality in combination with desired mechanical properties, are primarily formed by cold extrusion or cold drawing [1, 4]. Non-circular drawn products make up only about 15% of the total production of drawn products. Non-circular drawn products can be categorized based on the type of cross-sectional profile into those with regular or irregular polygonal sections, flat or flat-oval sections and special sections. Wires with a cross-section close to square, with concave walls or twisted profiles along their own axis, are used for the production of nails for joining wooden elements or roller guides [5]. Square brass, aluminum, and high-alloy steel wires, ranging in size from 3 to 12 mm, are used for the production of bent elements, including household appliances, equipment for large retail stores, and precision machinery. Coils for magnets that generate strong magnetic fields are made from square and rectangular wires of Cu-Ag alloys [6]. For springs, elliptical wires have evolved [7]. Hexagonal-section wires are used as raw material for the production of hexagonal-headed screws or bolts and nuts, as well as the wrenches for them. Their production utilizes corrosion-resistant ferritic, ferritic-martensitic, and martensitic steels. They are supplied in softened, polished, semi-hard or hard conditions. Wide scope of application fields, however, is not reflected by quantity of scientific papers, and despite the differences in their properties and manufacturing process compared to round bars [8], studies on this subject are relatively scarce.

The properties of these products mainly depend on the parameters of the semi-finished drawing process and the degree of deformation in individual passes in reaching the final profile. Thus, the final strain gradient depends on proper selection of consecutive

Corresponding author: pskubisz@agh.edu.pl

https://doi.org/10.2298/JMMB250717019R

reductions. Due to the fact that the deformation zones of a profiled die are more extensive, despite non-uniformity on the periphery, the distribution of the final strain is significantly more uniform on the cross-section than in round products. Therefore, non-round profiles are readily used and different wire-drawing techniques and tool configurations have evolved through decades. Acid resistant austenitic stainless steels are characterized by high plasticity, which enables deformation in low temperature range, making it possible to control strength-ductility trade-off through the strain hardening. As strain hardening behavior of these steels varies dependent on alloying elements content [6], alloy selection and control of strain enables producing variety of strength characteristics in cold drawn wires and rods. For instance, proper selection of unit reductions in drawing can bring about 8% increase in tensile strength. On the other hand, applying excessive unit drafts (order of 35%) can lead to overloading or rupture. Work hardening, by increasing the resistance to plastic deformation after passing through the die working zone, can cause dimensional discrepancies in the final product due to incomplete filling of the corners or may lead to wire breakage. Thus, range of reduction in drawing is restricted to relatively narrow window, which imposes physical constraints on achievable reduction, necessitating multi-pass increments in reduction to achieve assumed geometry and properties, and avoid failure. Excessive reduction, however the most favorable to increase strength and productivity, is limited by breakage hazard when plasticity margin is exceeded. Too low reduction, obviously, is not suitable for economy reasons, as complete finish of corners or fillets is harder to get.

Significance of multi-aspect quality issues of cold-drawn rods makes it a vital subject and many a scientific work is devoted to finding good balance between efficiency, produced strength increment and plasticity to control dimensional accuracy and physicochemical properties by cold drawing parameters [9-11]. In this respect, effect of the material quality, feedstock preparation and technology on the flow behavior and the resultant mechanical properties are studied, as well as further processing, such as thermochemical treatment, joining or in-service performance [12-15]. Beside experimental techniques and theoretical methods such as slab method [16] or upper bound method [17, 18] modeling with finite element method (FEM) [19, 20] or finite volume method [21] fuzzy logic and mathematical optimization [22, 23], equipotential lines and, most recently, AI have been used [24, 25]. The aspects prevailing in scientific papers are parametric estimation of the effect of operating parameters (e.g. friction and lubrication [26, 27], rate [28, 29], die profile [17, 30], and distribution of reduction division in multi-pass process [31, 32] on load [19], strain level [33, 34] and fill-out of corners and overall dimensional accuracy [7]. These problems are the basis for extension of numerical analysis into more advanced issues, such as failure prediction [19], [35], tool life aspects [36], and last but not least, strain-hardening related problems [37, 38], enabling mechanical properties assessment.

Strain hardening dependence on strain and process conditions has an apparent effect on the strength-ductility outcome of the cold-drawn products [39, 40] as well as on the deterioration of deformation capability to accommodate the desired reduction in multi-pass cold drawing, which are primary directions in the state-of-the-art of modelling of wire or rod cold drawing. This paper comes along with this line of research, investigating the limits in increasing reduction aimed at strain hardening while cold drawing acid-resistant austenitic steel X6CrNiTi18-10 when a non-round cross-section is to be obtained. To meet the expectation of productivity and desired hardening gradient and strain hardening increment, the highest possible reduction is favorable, limited by failure hazard. In the case of rod drawing, the both aims dovetail as increasing reduction favors both hardening and minimizing the number of drawing passes. Thus, the utilitarian goal of the study was a selection of conditions of the rod drawing process favorable for producing the required cross-section, featured by the best strain hardening profile and reduction of cross-sectional area being optimal, that is, as large as possible but not exceeding the drawing limit of the cold-worked material.

2. Materials and Methods

The work involved numerical analysis and experimental tests of the rod drawing process using varied starting diameters, resulting in different reduction ratios, which were carried out for final geometries, square and hexagonal. A varied reduction ratio (z) was meant to indicate the capability of attaining satisfactory quality polygonal cross-section rods that feature the best fill-out of corners and uniformity of strain hardening with simultaneous considerable load and plasticity.

For the two geometries included in the study (Fig. 1a, b), initial rod diameters were selected in a way that provided a consequent increase in the reduction ratio, starting with commercially available diameters for square and preparing diameters which produced comparable reduction ratios between square and hexagonal cross-sections. That means, the initial rod diameter and die profile were chosen so that, when using a square die, the resulting reduction closely matched that applied in a hexagonal die, e.g. S1 with H1, etc. (Tab.1). This approach enables similarity of

reduction for consistent analysis of the material's properties across various die types and rod dimensions. The reduction ratios were selected considering limits imposed by the available load of a laboratory rod-drawing stand installed on an Instron testing machine (Fig. 1c), based on theoretical load F_{dr} calculated after Siebel (1). According to Siebel, the drawing force can be calculated with the following equation

$$F_{dr} = A_1 \cdot k_{str_m} \cdot \varphi_p \left(\frac{\mu}{\alpha} + \frac{2 \cdot \breve{\alpha}}{3 \cdot \varphi_p} + 1 \right) \quad (1)$$

valid for friction coefficient values from μ = 0.02 to 0.05 [41]. In this calculation the mean coefficient of friction is μ = 0.035. The optimum drawing angle, requiring the least force, is around 2α = 16°. From this it follows for the angle in radians:

$$\breve{\alpha} = \frac{\pi}{180°} \cdot \alpha° = \frac{\pi}{180°} \cdot 8° = 0.13 \quad (2)$$

If these values are brought into the above equation, then the approximate drawing force can be determined with the simplified equation:

$$F_{dr} = \frac{A_1 \cdot k_{str_m} \cdot \varphi_p}{\eta_F} \quad (3)$$

where:

F_{dr} (in N) - the drawing force; k_{strm} (in N/mm^2) - mean flow stress; A_1 (in mm^2) - cross-section of the wire after drawing; φ_p - principal strain ($\varphi_p = \ln (A_0/A_1)$); n_F - deformation efficiency.

To compensate for the redundant work of plastic deformation, related to the lateral flow into corners of the polygonal cross-section, the formula was modified by supplementing it with a shape factor k to obtain:

$$F_{dr} = k_{str_m} A_1 \left(1 + \frac{\mu}{\mathrm{tg}\alpha} \right) (1 + kz) \quad (4)$$

A_1 – final cross-sectional area of the drawn rod; k_{strm}– mean flow (yield) stress value; μ - friction coefficient between the material and the die; α - half-angle of the conical die; k - shape factor for considering effect of redundant deformations (for square: k = 1.1, for hexagon: k = 1.15); z – reduction ratio, calculated as

$$z = 1 - \frac{A_1}{A_0} \quad (5)$$

A_0 – initial cross-sectional area of the rod to be drawn.

The materials subjected to drawing were round rods, varied in diameter, made of austenitic acid-resistant steel X6CrNiTi18-10 (1.4541, AISI 321) of chemical composition presented in Tab. 2, featuring an average Vickers hardness (HV) of 158.4 HV.

Table 1. *Geometry and load parameters of drawing schemes assumed in the study*

Drawing scheme	Feedstock diameter	Area reduction, (z)	Drawing load, F_{dr}
	mm	%	kN
S1	20	37.6	73.1
S2	18	23	65.4
S3	17	13.7	60.4
H1	18.6	37.5	69.1
H2	16.8	23.5	43.1
H3	15.8	13.5	24.7

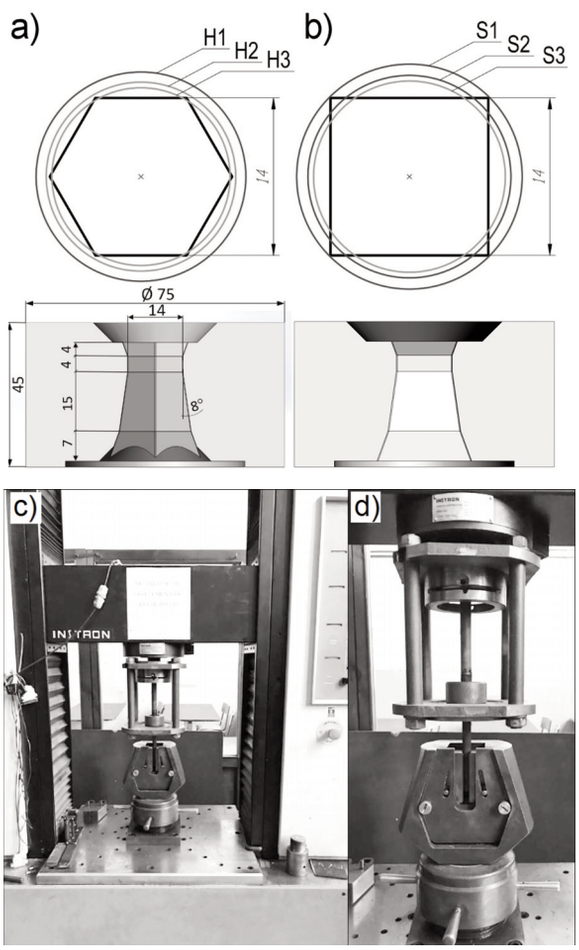

Figure 1. *Experimental details: geometries of hexagonal (a) and square (b) drawing dies applied in the experiment with designation system used for analyzed cases of initial rod variations, c) laboratory rig installed in Instron testing machine, d) the drawing stand*

Table 2. *Chemical composition of X6CrNiTi18-10 steel used in the study*

Element content, wt%													
C	Si	Mn	P	S	Cr	Ni	Mo	Ti	Cu	Al	Co	Nb	V
0.09	0.31	1.84	0.034	0.013	17.9	10	0.34	0.41	0.18	0.03	0.06	0.02	0.04

Numerical modeling of the process was conducted in commercial code QForm3D, which has proven reliable in similar stationary process FEM simulation [16, 42]. Geometry of a quarter of full shape was used with definition of symmetry planes in half of planes perpendicular to rod radius. Numerical model was based on tetrahedral mesh with 9 Gauss integration points, varying from 5 to 8 elements on a radius, densified correspondingly to gradient of solution by automated algorithms of adaptive remeshing. Elastic-plastic model of deformed body was assumed for drawn rod. Friction conditions were defined by Levanov model with friction factor 0.15 to correspond with the experiments (soap solution). Drawing velocity of 20 mm/s was assumed.

Material characteristics was described with Hensel-Spittel formula (6) with coefficients determined by means of multiple regression of the experimental data derived from uniaxial compression tests of the wire in as-received condition [43-45]. The values of flow stress were obtained from the load-displacement functions undergone inverse method processing to compensate for heat generation. The coefficients are set in Table 3.

$$\sigma_p = Ae^{m_1 T}\varepsilon^{m_2}e^{m_4/\varepsilon}\dot{\varepsilon}^{m_3} \tag{6}$$

Table 3. *Coefficients of Hensel-Spittel equation assumed in FEM simulation of drawing*

Parameter	Value
A	1392
m_1	-0.0011
m_2	0.14811
m_3	0.00933
m_4	0.00134

3. RESULTS

3.1. Assumptions and the parameters of interest in FEM simulation

In the cold wire- and rod-drawing process, the total strain comprises plastic (permanent) and elastic (non-permanent) strain, which is released as the drawing is complete. For practical engineering applications, equations used in modeling should encompass both components, represented by their respective strain tensors. For the total strain produced during the reduction of a rod, resulting from its initial dimensions and die cross-section, described as a sum of elastic and plastic parts:

$$\varepsilon = \varepsilon^e + \varepsilon^p \tag{7}$$

where: ε – total strain tensor, ε^e – elastic strain tensor, ε^p – plastic strain tensor.

The elastic strain tensor, ε^e, relates to the reversible part of the deformation. It is associated with the stress tensor by Hooke's law, which for linear isotropic materials reads:

$$\varepsilon^e = \frac{1+\nu}{E}\sigma - \frac{\nu}{E}tr(\sigma)I \tag{8}$$

where: E – Young's modulus, ν – Poisson's ratio, σ – Cauchy stress tensor, I – identity tensor, tr(σ) – trace of the stress tensor, representing the volumetric part of stress.

The plastic strain tensor, ε^p, describes the irreversible part of deformation, which produces permanent final dimensions of the drawn rod. A commonly used relation for plastic flow of isotropic materials is:

$$d\varepsilon^p = d\lambda\frac{\partial f}{\partial \sigma} \tag{9}$$

where: $d\varepsilon^p$ – increment of plastic strain, dλ – scalar multiplier (plasticity parameter), ∂f – the yield function, e.g. $\partial f = \sigma_{eq} - \sigma_y$, where σ_{eq} is the equivalent stress (effective stress) and σ_y is the yield stress. The equivalent strain is a scalar measure of the strain state used in engineering to compare multiaxial strain to uniaxial strain, producing equivalent output. It can be defined using the deviatoric strain tensor, which refers to the component of the strain tensor responsible for shear strain:

$$\varepsilon_{eq} = \sqrt{\frac{2}{3}\varepsilon^d : \varepsilon^d} \tag{10}$$

where: $\varepsilon^d = \varepsilon - (1/3)tr(\varepsilon)I$ is the deviatoric part of the strain tensor, and the colon operator denotes the double dot product of a tensor (contraction over two indices). In case of strains conforming to linear strain theory (small, or quasi-linear), the equivalent strain can be directly related to the components of the strain tensor in the chosen coordinate system.

On account of the significant importance of elastic strain in a cold drawing process, the modeling of this process involves an elastic-plastic model of a

deformed body. Thus, numerical estimation of the total strain produced in drawing an individual round cross-section into a polygonal cross-section takes into account both components, elastic (Fig. 2a) and plastic (Fig. 2b), which can be defined, respectively,

$$\varepsilon_{eq}^{e} = \sqrt{\frac{2}{3}\varepsilon^{e} : \varepsilon^{e}} \text{ and } \varepsilon_{eq}^{p} = \sqrt{\frac{2}{3}\varepsilon^{p} : \varepsilon^{p}} \tag{11}$$

For the quantitative relation between strain and hardness, permanent strain is boiled down in this study. As a well-established parameter commonly used for the description of deformation, equivalent strain is used in this study as a measure of the amount of strain:

$$\varepsilon_{eq} = \sqrt{\frac{2}{3}\left[\varepsilon_{11}^{2} + \varepsilon_{22}^{2} + \varepsilon_{33}^{2} - \varepsilon_{11}\varepsilon_{22} - \sqrt{-\varepsilon_{22}\varepsilon_{33} - \varepsilon_{33}\varepsilon_{11} + 3\left(\varepsilon_{12}^{2} + \varepsilon_{23}^{2} + \varepsilon_{31}^{2}\right)}\right]} \tag{12}$$

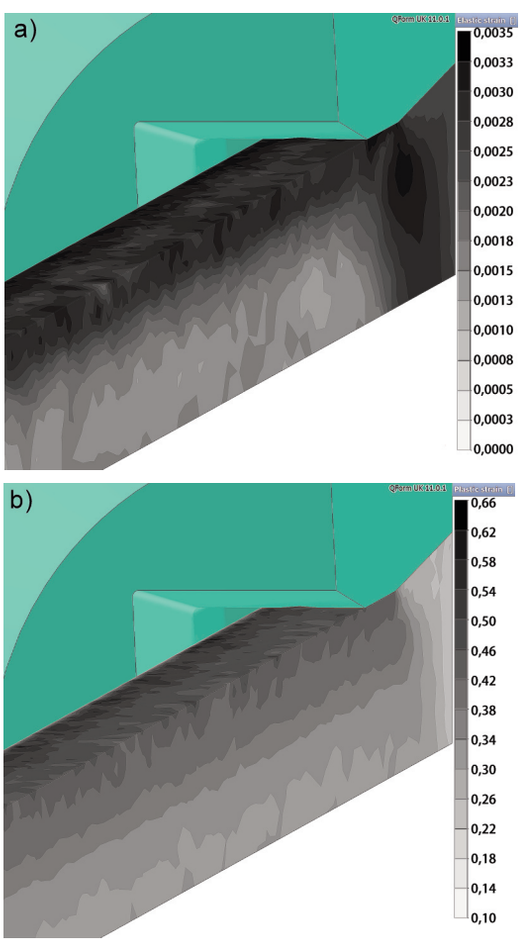

Figure 2. *Longitudinal cross-cut distribution of: a) elastic strain, b) plastic strain of the square rod*

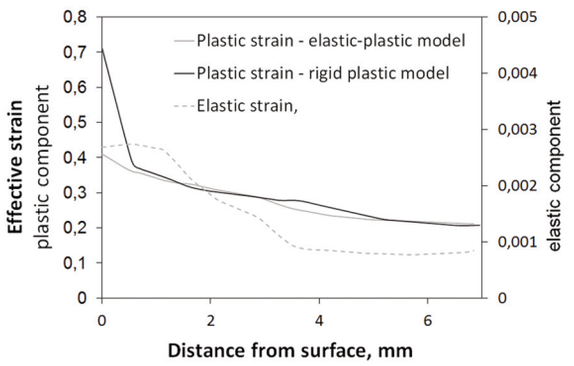

Figure 3. *Numerically estimated level of plastic and elastic strain in rigid-plastic and elastic-plastic model of deformed body assumed in FEM simulation*

In the context of the work, of primary importance is the plastic strain component, which results from imposed reduction ratios, and is of significance for the interpretation of hardness measurements or the validation of FEM models, e.g. drawing load plots compared with experimental load plots. From the strain hardening standpoint, the permanent strain component is of primary importance, so the focus is on plastic effective strain (9), and it will be included in the analysis as a determinant responsible for producing as-drawn mechanical properties. However, to take the accompanying effect of elastic strain on the actual amount of deformation (Fig. 3), for the credibility of the FEM calculations, an elastic-plastic model of the deformed body was assumed in the simulation.

3.2. Results of FEM modeling

Numerical modeling allowed quantitative investigation of strain and its distribution on the cross-section depending on applied initial diameter and resulting reduction. As expected, increasing reduction produces increasing level of effective strain and unit pressure on tool, which causes increasing drawing load. As a representative universal measure of amount of plastic strain, effective strain distribution produced in the realized drawing cycles is shown in Fig. 4 and Fig. 5.

Whereas the maps illustrate the strain profile throughout the deformation zone and run-out drawn rod, for more accurate quantitative analysis effective strain in the surface and the axis was plotted (Figs. 6 and 7). On account of fluctuation of solution between Gaussian integration points, typical of FEM output, regression was made for reasonable interpretation. Except for S1 – the highest reduction which turned out excessive in physical and numerical effort and has not managed to reach the stage of stable strain level (Fig. 6a), analysis of all remaining trials is described with coefficients of a linear function y = ax + b.

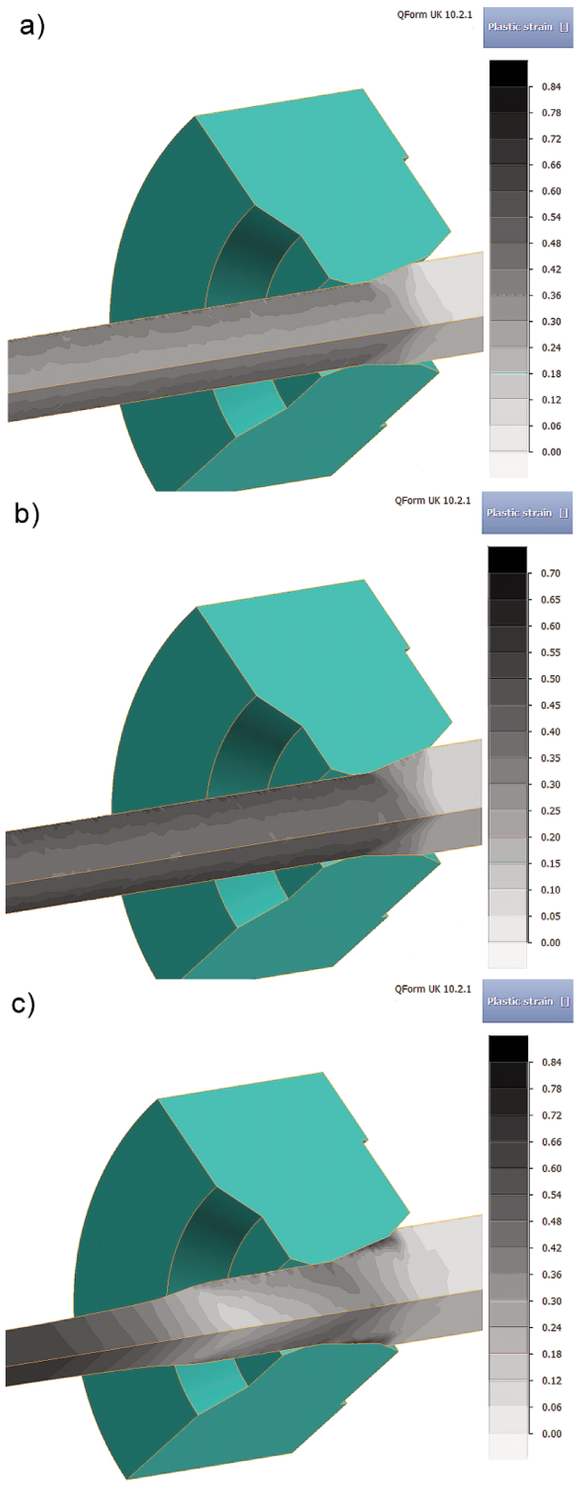

Figure 4. *FEM calculated effective strain in drawing schemes S1-S3 of square rods on the longitudinal cross-section (a-c)*

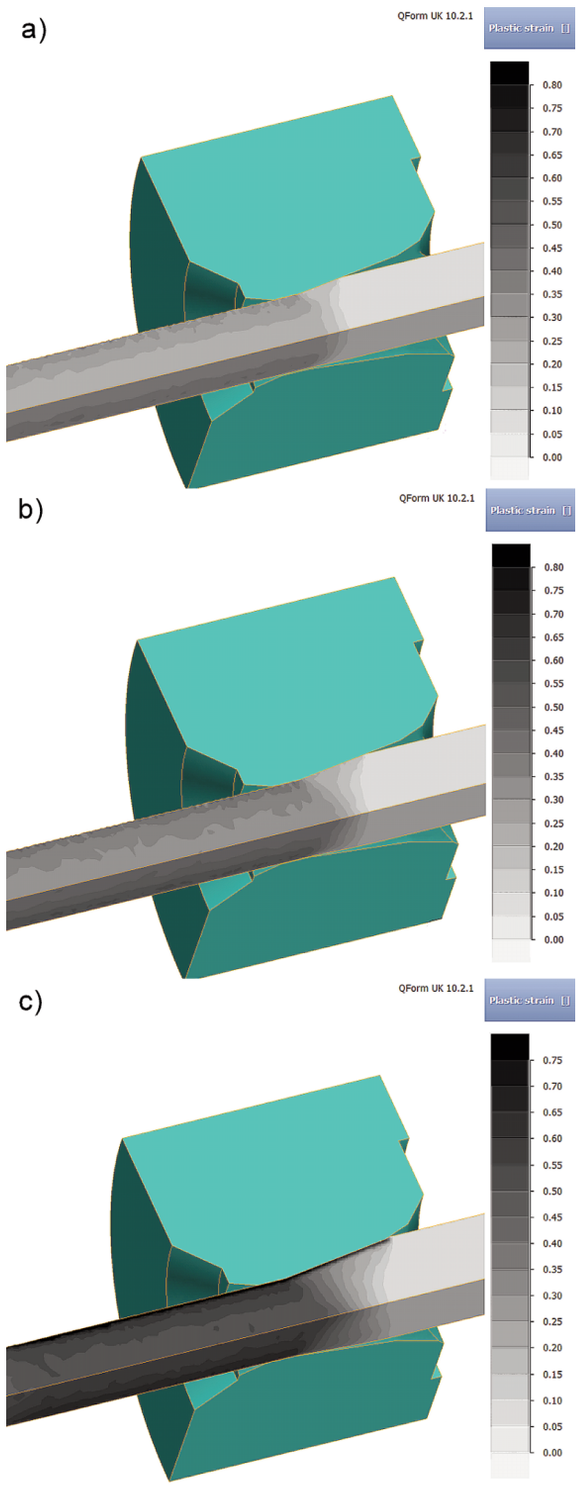

Figure 5. *FEM calculated distribution of effective strain in drawing schemes H1-H3 of hexagonal rods on the longitudinal cross-section (a-c)*

The value of b is an average from 50 readout points along representative length of a drawn rod, and the scalar representation of strain. The comparison of numerically calculated (Fig. 8) and experimental

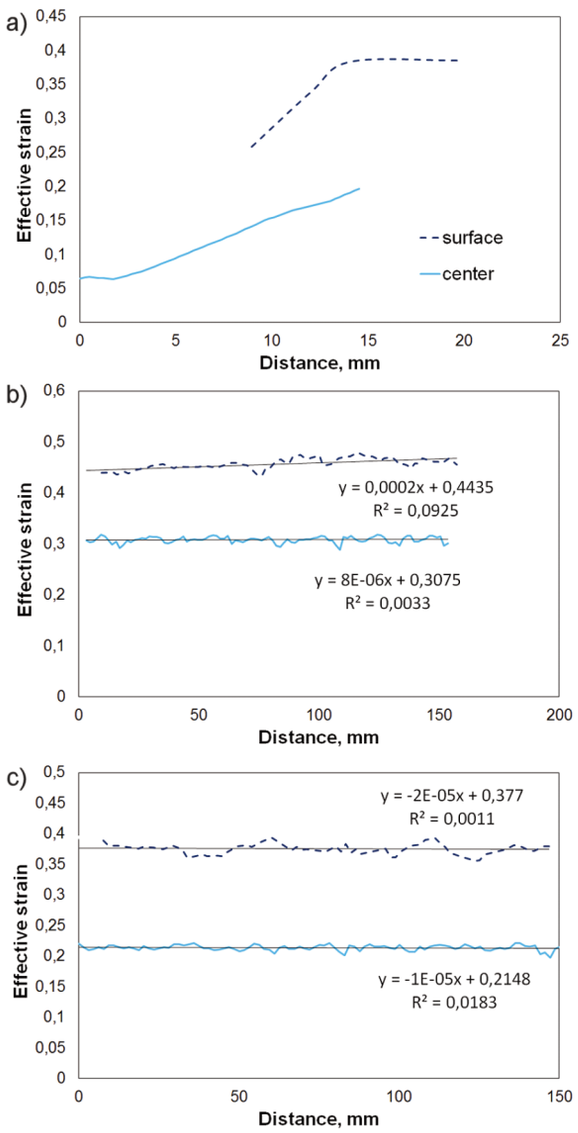

Figure 6. *FEM calculated effective strain in drawing of square rods, on the surface and the axis with linear regression, where a)-c) denote S1-S3, respectively*

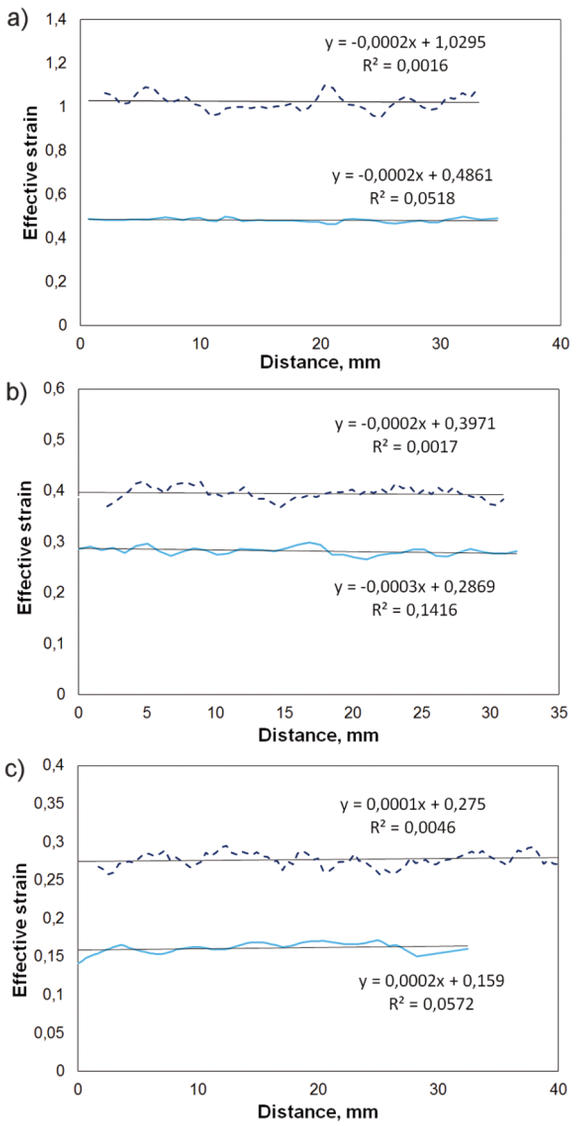

Figure 7. *FEM calculated effective strain in drawing of hexagonal rods, on the surface and the axis with linear regression, where a)-c) denote H1-H3, respectively*

drawing force plots indicate very good agreement (Fig. 9). Serving as validation of the models, it speaks for credibility of the whole of the conducted simulations and thereby obtained strain distribution and reliability of the information derived from the determined distributions of equivalent strain across the cross-section and along the length of the rods.

3.3. Evaluation of the quality of the experimental samples

3.3.1. Dimensional accuracy

The assumed initial billet diameters influence the variation in the reduction ratio among the selected combinations of billet and product geometries. Excessive reduction has resulted in failure for samples S1, S2, and H1. Quality inspections of the successful experimental samples (S3, H2, and H3) allowed us to estimate dimensional accuracy, specifically the alignment of the dimensions of the produced rods with the assumed dimensions.

This comparison reveals that as the reduction ratio increases, the underfilling of the corners tends to increase as well, as illustrated in Fig. 10a) to c), which shows black-field macrographs of polished sections alongside theoretical geometries (contour lines). It

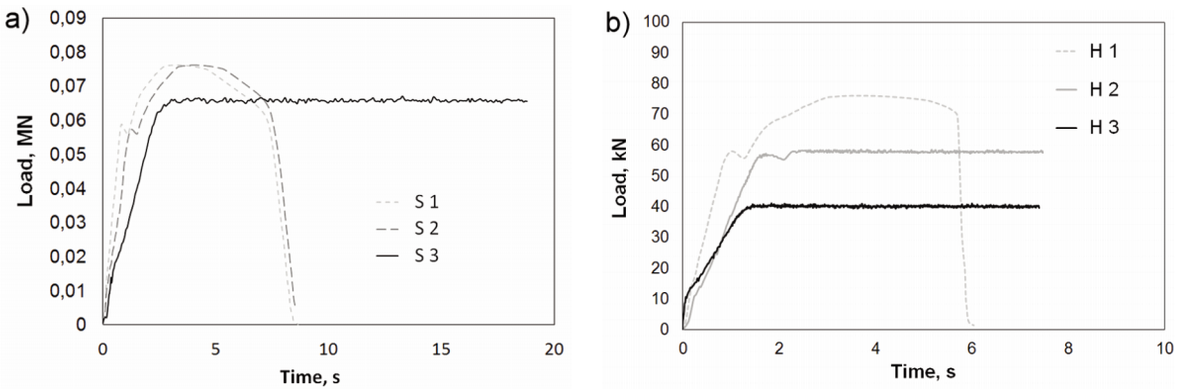

Figure 8. *FEM calculated drawing load: a) square rods, b) hexagonal rods*

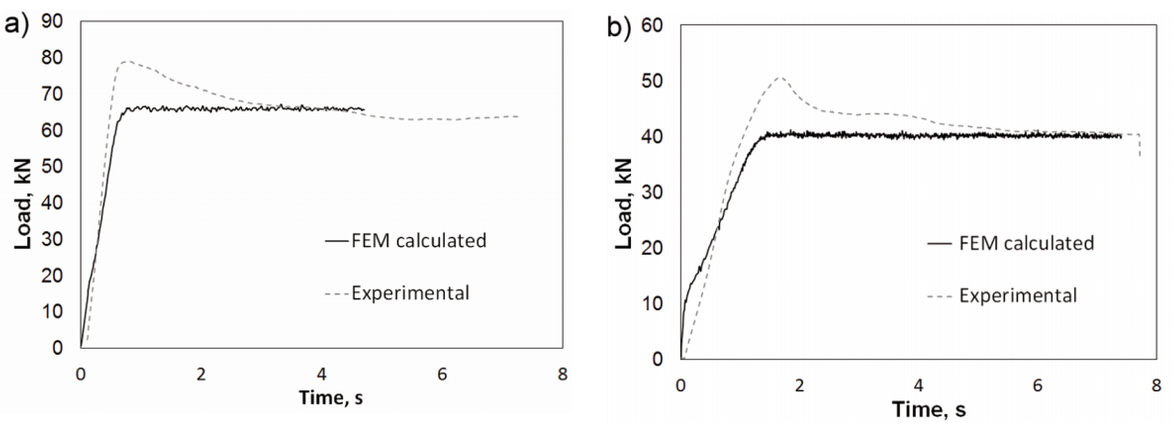

Figure 9. *Comparison of FEM calculated and experimental drawing load: a) square rod S3, b) hexagonal rod H3*

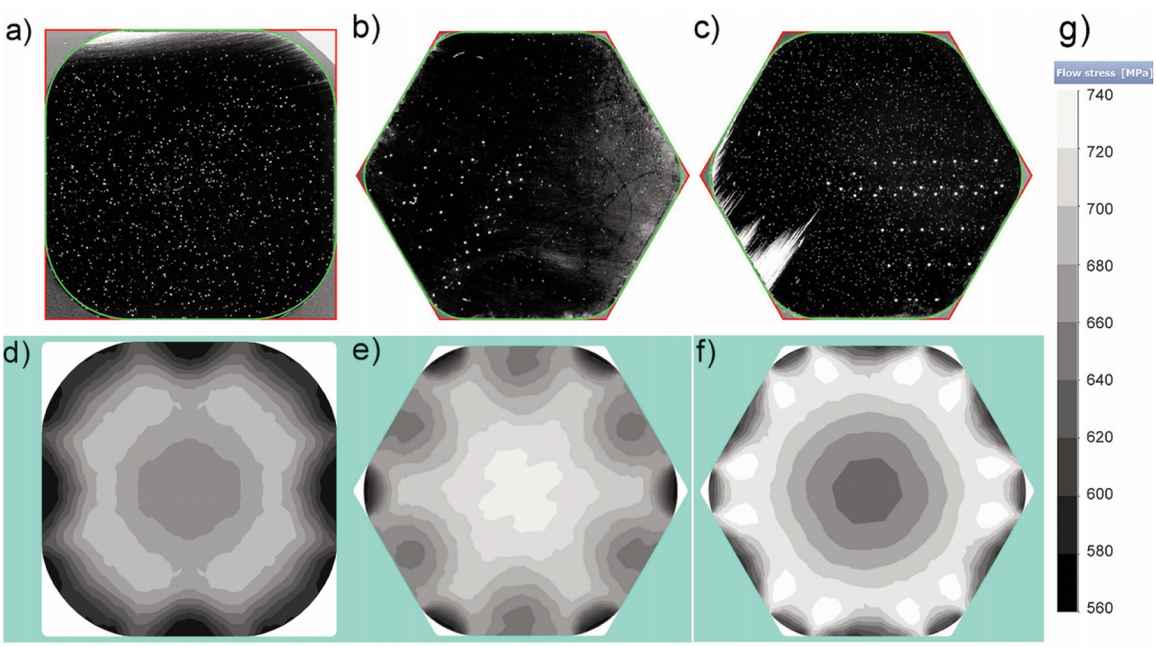

Figure 10. *Fill-out of corners represented by theoretical (assumed) and actual cross-sections of experimental samples of: a) square rod S3, b) hexagonal rod H2, c) hexagonal rod H3 and, respectively, d)÷f) FEM calculated cross-sections in the half of the length of calibrating section of drawing die, on the background of flow stress distribution with legend (g)*

Table 4. *Comparison of underfilling produced in the drawing process on the basis of theoretical and planimetrically estimated cross-sections*

Sample	Cross-sectional area after drawing, mm^2		Underfilling, %
	Theoretical	Actual	
S3	195.31	185.66	4.94
H2	169.42	166.74	1.58
H3	169.42	165.68	2.21

becomes clear that not only can a reduction that is too small lead to issues, but a reduction that is too large can also cause insufficient filling of the corners. This finding may be surprising, given the expected relationship between reduction and drawing load.

By comparing experimental measurements with theoretical assumptions, we can assess the degree of underfilling in the actual cross-section by subtracting the final cross-section from the theoretical one (see Tab. 4). The same analysis can be applied to numerically estimated cross-sections. FEM calculated cross-sections at the midpoint of the calibrating section of the drawing die align with the experimental evaluations. The flow-resistance-related origin of the underfilling is confirmed through numerical simulations (see Fig. 10d-f). The results show a consistent amount of cross-section that remains unfilled by the metal being shaped into the polygon, along with a slight increase in the gap with higher reductions. Interestingly, while the initial geometry is closer to the final shape at higher reductions, the cross-sectional area in Fig. 10e) is notably larger than in Fig. 10f). There is no single standard to prop on while estimating the efficiency of the fillout of the corners in a single pass, thus, the results of the fillout assessment are mostly of comparative meaning. However, it contributes to overall efficiency of the multi-pass process, minimizing total number of drawing runs, which translates into productivity, tool life and fixed cost of maintenance.

Additionally, it is essential to note the pattern of flow stress concentration and gradient in each of the compared output maps of flow stress (presented at the same scale in Fig. 10 g). As the reduction increases, the penetration of the stress zone becomes deeper, and significantly higher flow stress values are observed for the same reduction.

3.3.2. Hardness measurements

The hardness measurements for the successfully drawn rods are presented in Figures 11 to 13. Each analyzed sample shows a reasonable gradient of hardness in both the longitudinal direction, with hardness increasing as strain rises (see figure b), and

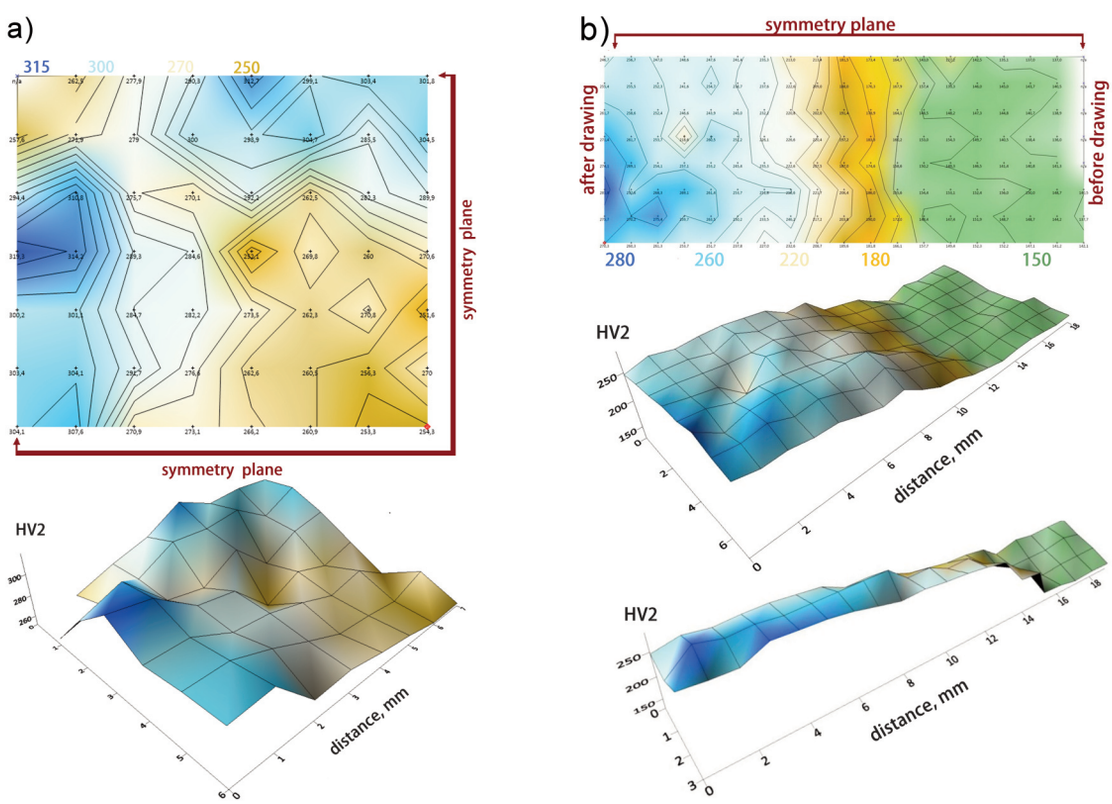

Figure 11. *Hardness distribution of cold drawn square rod S3 on a) transverse, b) longitudinal cross-sections*

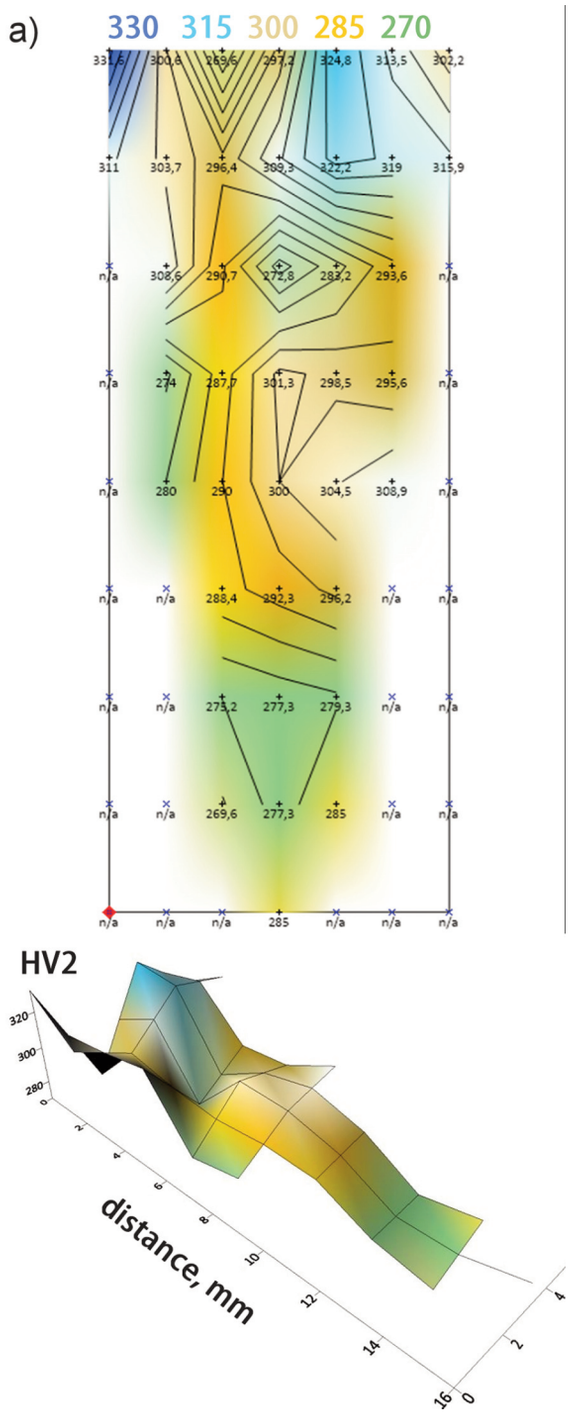

across the transverse cross-section (see figure a), where hardness varies from the axis to the surface due to strain distribution caused by geometry-induced deformation zones.

As strain increases, there is a corresponding rise in strain hardening, which is confirmed by the hardness measurements. However, it is somewhat surprising that the corners of the rods, which experienced the highest reductions, showed slightly lower hardening. Planimetrical measurements of the cross-sectional area indicate that excessive reduction during the drawing of austenitic steel rods has its limitations.

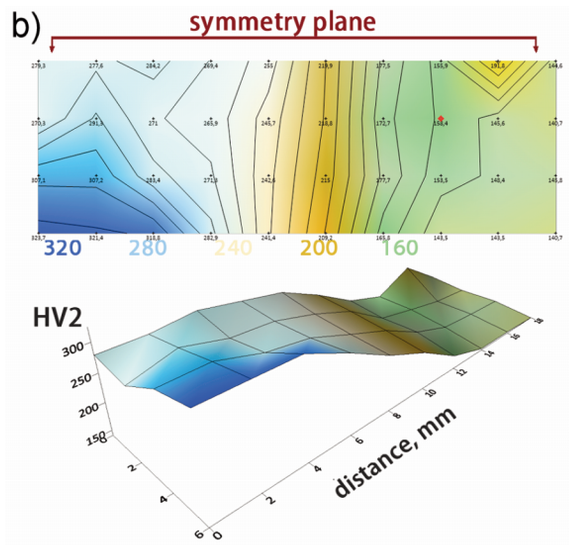

Figure 12. *Hardness distribution of cold drawn hexagonal rod H2 on a) transverse, b) longitudinal cross-sections*

Unlike round rods, which have axial symmetry along their length, square and hexagonal cross-sections possess mirror-like symmetry. This results in non-uniform strain distribution circumferentially, which is different from that in circular rods. Strain concentrations occur at the center of each side of the polygonal cross-section, leading to areas of locally higher strain-induced hardness enhancement. Consequently, cold-drawn rods exhibit a heterogeneous increase in strength, accompanied by a simultaneous deterioration in ductility.

The strain hardening effect, which is the expected result of increased reduction, also leads to a decrease in plasticity and corner fill-out levels. This limitation must be considered when selecting high reduction rates for the drawing processes of polygonal rods made from acid-resistant austenitic steel, necessitating a revision of the design principles for drawing schemes for these products.

The results of the tests are summarized in Table 5, which compares the numerical modeling results with the experimental test outcomes. It is evident that both insufficient and excessive reductions—due to various reasons—can result in incomplete filling of the corners. To accurately interpret the predicted forces and hardness levels in relation to the actual reductions, one must account for the incomplete filling of the corners that results from increased hardening and the larger die-contact frictional area. This indicates the need for a tailored selection of the

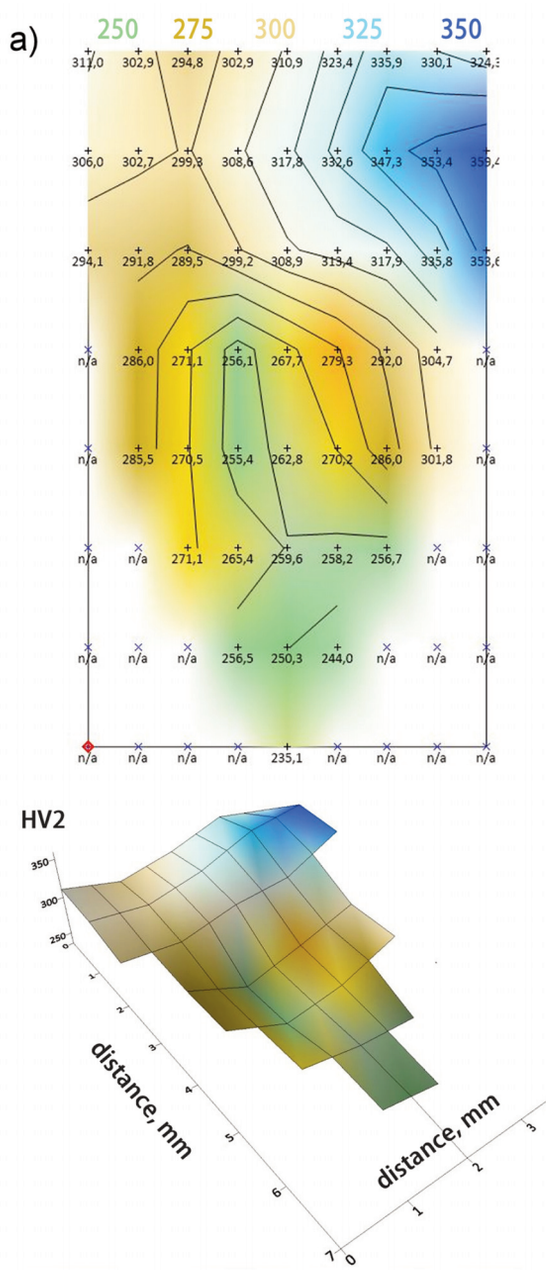

Figure 13. *Hardness distribution of cold drawn hexagonal rod H3 on a) transverse, b) longitudinal cross-sections*

reduction degree for specific rod cross-sections and the material's hardening characteristics.

4. Evaluation and Discussion

The drawing scheme—whether round to square or round to hexagonal—significantly impacts the produced strain distribution and resultant strain hardening. Analyzing the material flow in each of the examined cases, it is evident that with the progression of drawing, the hardness of the material increases with greater strengthening corresponding to increasing reduction. The reduction ratio resulting from the feedstock diameter affects the depth of the deformation zones' penetration towards the axis, and the resulting hardness of the rod; the larger the diameter, following the principle that the higher the strain and the hardness. The presented results, however, tend to show that this direct relationship has

Table 5. *Summary of the experimental and FEM modeling results of cold drawing study*

Sample	Effective strain (ε)			Hardness, HV[1)]		Load, kN		[1)] Hardness measured on transverse cross-section [2)] N.d. – no data; hardness was not measured as a representative drawn length was not reached [3)] The maximum of the load reached before failure [4)] Arithmetic average from FEM calculated values within stable process
	Surface	Axis		Axis	Surface	FEM[4)]	Exp.	
		FEM	Theoretical / True					
S1	0.384	0.22	0.472 / -	n.d. [2)]	n.d. [2)]	76.26	82[3)]	
S2	0.443	0.3075	0.261 / -	n.d. [2)]	n.d. [2)]	76.18	80[3)]	
S3	0.377	0.2148	0.147 / 0.201	251	315	64.19	63	
H1	1.029	0.4861	0.471 / -	n.d. [2)]	n.d. [2)]	76.17	82[3)]	
H2	0.398	0.2869	0.267 / 0.285	285	331	57.8	54	
H3	0.275	0.159	0.145 / 0.168	235	359	40.6	40	

its limits. In case of the considered polygonal rods, circumferential irregularity of strain resulting from the non-round deformation zone, affects the depth of the deformation zones' penetration towards the axis. Additionally, the substantial differences in cross-sectional geometries between the feedstock and cold-drawn rods mean that the actual reduction ratio may vary from the theoretical estimates based on cross-section ratios. These findings suggest reconsidering design practices while choosing the reduction ratio for cold drawing polygonal rods.

Facilitating numerical modeling has enabled a theoretical analysis of metal flow phenomena within the deformation zone during rod reduction. The simulations showed that the computational results can deviate significantly from initial assumptions with increasing reduction per pass. Metal flow phenomena, such as corner underfilling and friction elongation, which vary along the length of the die orifice during drawing, make FEM an effective tool for simulating the drawing of rods with polygonal cross-sections. The FEM simulation results confirmed that the observed efficiency of reduction—specifically issues related to underfilling—is a consequence of axial-lateral metal flow interactions, rather than random process conditions anomalies. Although it takes multi-pass drawing sequence to achieve the complete corners' fill-out and dimensions of polygonal rods, the effect of cross-sectional reduction on the achieved die-corners fillout rate has a bearing on the number of passes and ultimate productivity. The results show that applying a multi-pass schedule is indispensable to produce completely shaped corners. Increasing the reduction to minimize the number of passes may lead to excessive hardening, which hampers the lateral flow of the metal towards the corners and increases the drawing force and failure hazard.

Despite applying similar reduction values, samples S3 (square) and H3 (hexagon) exhibited considerably different drawing force values. The highest drawing force recorded was approximately 63 kN for sample S3, while sample H3 exhibited the lowest force at about 40 kN. Notably, the actual reduction achieved during the rod drawing was slightly higher than the theoretical reduction, as the material inadequately filled the corners of the square-section and hexagonal-section dies. This discrepancy can be attributed to a relative similarity of cross-sections, which leads to two factors related with shape factor. The more obvious one – dissimilarity of the frictional area in the deformation and calibration zones of the die. The other one can be referred to as dissimilarity of a trajectory of any material point located beside any of the symmetry planes, which can be traced back to redundant strain associated with accommodating fillout of the corners. This phenomenon, not present in drawing round rods or wires, contributed to discrepancies between hardness profiles in and out of the symmetry planes and well as in the drawing force estimation. In this aspect, introducing of redundant-strain-related shape coefficient supports agreement of the load calculation for cold-drawing any of the non-round rods. Except for the peak stage, the estimation error between the calculated and measured steady-state value of the drawing load does not exceed 4.5% and 3.5% for square and hexagonal rod, respectively. Assuming no additional frictional effects, this suggests a potential design consideration: closer geometrical similarity might improve the efficiency of the drawing process. As long as the values of the shape factor k are satisfactorily validated, this finding can bring significant and time-saving aid for drawing load consideration in design of cold drawing of irregular cross-sections of rods which takes much time when modeling with incremental methods, such as FEM.

In addition to load estimation, the other aspect of the study intended to provide utilitarian results is the hardness correlation to the imposed reductions. The successfully completed drawing experiments allowed for measuring hardness and creating a hardness gradient profile for the square and hexagonal rods produced from round rods through varying reductions. The maximum hardness levels reached up to 360 HV, which aligns with many related studies that indicate a cold-work-induced hardness level ranging from 203 HV to 266 HV. However, it is not only the value that counts while predicting the mechanical properties; equally important is the prediction of the profile of hardness, which has a bearing on its uniformity. Mapping hardness across the cross-section provides an experimental illustration of strain distribution for both geometries, including the depth of the deformation zone and uniformity of properties within a rod.

A detailed analysis of strain and hardness distribution underscores the practical significance of strain hardening in producing targeted hardness by controlling reduction ratios on consecutive passes. The obtained hardness level aligns with the results of similar study of the twin grade 304L [38, 45] and the literature data for wire-drawing and other cold-deformation-based metal forming processes in reference to the studied alloy. In this regard, this study comes along with references to the hardness of X6CrNiTi18-10 steel appearing in related works [46, 47]. Focusing on the works aimed at the pursuit of increased hardness, [48, 49] reports exceeding 500 HV for thin wires and, starting from about 270 HV, fine-grained material cold-drawn at high speeds. However, for conventional material, referred to as coarse-grained, the achieved hardness is 490 HV for initial hardness over 180 HV. This work's results should also be confronted qualitatively with detailed

analyses of the effect of a strain gradient on the hardness profile of the cold-drawn wires or rods. For instance, in the study by [50], a sudden sub-surface drop from 474 HV in the surface to 228 HV, not deeper than half a millimeter below. Here, for hexagonal rods, the surface hardness 336 HV drops to 305 HV and for the square one, it takes half of the radius to descend from 280 HV to 240 HV. It allows us to conclude that, despite an irregular pattern on the periphery, the hardness gradients of the polygonal cold-drawn rods are smaller and the hardness is more uniform on the cross-section.

Combined with quantitative analysis, this mapping offers a method to control the property gradient of square and hexagonal rods made from acid-resistant steel X6CrNiTi18-10, providing reliable data for feeding artificial intelligence models. The experimental hardness values correlate well with the effective strain obtained from simulations, confirming the reliability of FEM in predicting property gradients.

Failures in some samples (S1, S2, H1) indicate a limit to drawability at the imposed reductions, as these drawn rods broke during processing. It is important to note that the steel was delivered in a supersaturated condition, which had improved its ductility. However, for the imposed reduction ratios, the ductility was insufficient to enable the drawing process, even with moderate strain rates. Attempts to reduce the drawing speed (below 10 mm/s) and apply additional lubrication did not alleviate the issue. The stress required for deformation in these cases exceeded the tensile strength of the material, resulting in failure. This highlights that optimizing the drawing process parameters for polygonal rods ultimately involves striking a delicate balance between achievable cross-section reduction and drawing limits. Excessive reduction can lead to a disproportionate increase in load and unit stresses on the tool relative to the reduction, leading to decreased plasticity margin of the worked rod. Conversely, an appropriate level of reduction is crucial to achieve the desired hardness profile through strain hardening. Improperly high decreases can lead to flow instability and failure, increased resistance to deformation, and complications related to corner fill-out. Thus, two concurrent factors must be considered to optimize the drawing process.

5. Conclusions

The studies on drawing square and hexagonal rods with variable reduction ratios demonstrate that, despite their geometric similarities, the process of drawing polygonal wires and rods is relatively complex. This complexity arises from the non-uniformity of deformation, leading to differing work hardening and changes in plasticity. The results can be summarized in the following key conclusions:

1. The drawing scheme and reduction ratio significantly influence strain distribution, hardness, and drawability limits. The transition from round to square or hexagonal sections notably affects material flow and strain hardening. While increased reduction typically enhances hardness, excessive reduction can lead to a loss of plasticity and ultimately rod failure, establishing clear limits on feasible deformation. Material limitations indicate that even solution-treated X6CrNiTi18-10 steel did not sustain higher reductions despite adjustments in the drawing speed.

2. The discrepancy between the theoretically predicted and the actual cross-section underscores the necessity for design adjustments. Due to incomplete corner filling and shape mismatches, the actual reduction ratios often differ from those calculated geometrically. This difference impacts the drawing forces and strain predictions, indicating a need to revise conventional assumptions when designing dies for polygonal sections. The results show that applying a multi-pass schedule is indispensable to produce full corners. Increasing the reduction to minimise the number of passes may lead to excessive hardening, which hampers the lateral flow of the metal towards the corners and increases the drawing force and failure hazard.

3. Finite element modeling (FEM) reliably reproduced experimental trends, confirming phenomena such as corner underfilling, increased flow resistance, and stress–hardness gradients, thus validating FEM as an effective predictive tool. These simulations facilitate accurate predictions of metal flow phenomena, which can otherwise lead to process inefficiencies. The agreement between simulation results and experimental load values supports the application of FEM in drawing process analysis and its relevance in design models. Hardness mapping and FEM-based strain analysis provide a useful basis for controlling property gradients in polygonal rods and for feeding AI models in process optimization.

4. Numerical modeling reveals that the impact of reduction ratio on underfilling and drawing force indicates limitations caused by strain-hardening-related flow behavior of the material being processed. While greater strain enhances hardness and mechanical properties, it also reduces ductility, which results in increased deformation resistance, potential tool overload, flow instability, and cracking. Therefore, process optimization must strike a balance between hardness improvements and the drawability limits associated with each rod geometry.

The study highlights the need for further detailed analysis of the relationship between reduction ratio and corner fill-out, as this phenomenon distinguishes the design of drawing processes for polygonal rods

from those for round rods.

Acknowledgments

Financial support of Polish Ministry of Science and Higher Education within statutory funds, research subsidy contract no. 16.16.110.663 is acknowledged.

Authors' contributions

M. Rumiński: conceptualization, methodology, investigation, data curation, original draft preparation, review and editing, project administration

P. Skubisz: methodology, software, investigation, validation, original draft preparation, visualization, editing and review

P. Micek: data curation, formal analysis, draft preparation and review

All authors read and approved the final version of the manuscript.

Data statement

All research data are included in the paper. Any additional data that support the findings of this study are available from the first author upon request. Numerical models are made available under 10.17632/zrn6m425yh.1

Conflict of Interest

The authors declare no conflict of interest.

References

[1] D. Peckner, I.M. Bernstein, Handbook of stainless steels, McGraw-Hill Book Company, New York, 1977.

[2] D. Bricín, H. Gilík, Surface structure analysis of X12CrNiMoV12-3 and X6CrNiTi18-10 steel samples processed by laser shot peening (LSP), MATEC Web of Conferences, 367 (2022) 00004. https://doi.org/10.1051/matecconf/202236700004

[3] E. Kantoríková, An influence of nitrogen corrosion on microstructural and mechanical features of the X5CrNi18-10 steel, Archives of Foundry Engineering, 24 (3) (2024) 69-75. https://doi.org/10.24425/afe.2024.151293

[4] L. Donati, B. Reggiani, R. Pelaccia, M. Negozio, S. Di Donato, Advancements in extrusion and drawing: a review of the contributes by the ESAFORM community, International Journal of Material Forming, 15 (3) (2022) 1-28. https://doi.org/10.1007/s12289-022-01664-w

[5] J.H. Kim, J.H. Park, K.S. Lee, D.C. Ko, K.H. Lee, Design of an intermediate die for the multi-pass shape drawing process, Materials, 15 (19) (2022) 1-14. https://doi.org/10.3390/ma15196893

[6] W. Głuchowski, J. Domagała-Dubiel, J. Sobota, Z. Rdzawski, J. Stobrawa, K. Marszowski, Analiza procesu ciągnienia drutów Cu-Ag, Hutnik Wiadomości Hutnicze, 80 (8) (2013) 530-533.

[7] A. Sasaki, M. Nakano, H. Takao, H. Utsunomiya, Pass-schedule design for non-circular wire drawing, Proceedings of the 14th International Conference on the Technology of Plasticity – Current Trends in the Technology of Plasticity, Mandelieu-La Napoule, France, 2023, pp. 407–417.

[8] S.K. Lee, I.K. Lee, S.M. Lee, S.Y. Lee, Prediction of effective strain distribution in two-pass drawn wire, Materials, 12 (23) (2019) 1-13. https://doi.org/10.3390/ma12233923

[9] M. Masoumi, S.E. de Oliveira, M. Paredes, Influence of cold drawing on phase transformation and tensile properties of FeCrMn austenitic stainless steel 201, Steel Research International, 96 (6) (2025) 1-12. https://doi.org/10.1002/srin.202400469

[10] H.C. Yang, F.Y. Hung, B.D. Wu, Y.T. Chang, Application characteristics of ultra-fine 15 μm stainless steel wires: microstructures, electrical fatigue, and ball formation mechanisms, Micromachines, 16 (3) (2025) 1-21. https://doi.org/10.3390/mi16030326

[11] A. Khaliq, M.A. Rafiq, H.T. Ali, F. Ahmed, S. Mehmood, J. Grandfield, S.A. Ranjha, Melt quality induced failure of electrical conductor (EC) grade aluminum wires, Journal of Mining and Metallurgy, Section B: Metallurgy, 53 (1) (2017) 75-81. https://doi.org/10.2298/JMMB151006030K

[12] L.Y. Saubanova, S.V. Diachenko, V.S. Loray, L.A. Nefedova, S.P. Bogdanov, N.A. Khristiuk, M.M. Sychov, Gas atomization of X6CrNiTi18-10 stainless steel powder for selective laser melting technology, Materials Science Forum, 1040 (2021) 172-177. https://doi.org/10.4028/www.scientific.net/MSF.1040.172

[13] K.C. Sahoo, K. Laha, Influence of thermal ageing on tensile-plastic flow and work hardening parameters of indian reduced activated ferritic martensitic steel, Journal of Mining and Metallurgy, Section B: Metallurgy, 59 (2) (2023) 217–229. https://doi.org/10.2298/JMMB221114019S

[14] Q. Xu, J. Zhu, Y. Zong, L. Liu, X. Zhu, F. Zhang, B. Luan, Effect of drawing and annealing on the microstructure and mechanical properties of 304 austenitic stainless steel wire, Materials Research Express, 8 (12) (2021) 1-14. https://doi.org/10.1088/2053-1591/ac44d6

[15] D. Bricín, Z. Špirit, H. Gilík, J. Kaufman, Effect of laser shock peening on the microstructure of P265GH steel and X6CrNiTi18-10 stainless steel dissimilar welds, Manufacturing Technology, 24 (1) (2024) 9-14. https://doi.org/10.21062/mft.2024.020

[16] S. Di Donato, M. Negozio, R. Pelaccia, B. Reggiani, L. Donati, Experimental, analytical, and numerical analysis of the copper wire multi-pass drawing process, Materials Research Proceedings, 41 (2024) 742-752. https://doi.org/10.21741/9781644903131-82

[17] S. Alexandrov, Y.M. Hwang, H.S.R. Tsui, Determining the drawing force in a wire drawing process considering an arbitrary hardening law, Processes, 10 (7) (2022) 1-14. https://doi.org/10.3390/pr10071336

[18] S.H. Zhang, X.D. Chen, J. Zhou, D.W. Zhao, Upper bound analysis of wire drawing through a twin parabolic die, Meccanica, 51 (9) (2016) 2099-2110. https://doi.org/10.1007/s11012-016-0363-9

[19] R. Badi, S. Bensaada, N. Tala-Ighil, N. Lebaal, Numerical analysis of the effects of incremental reduction rate in the wire drawing process, The International Journal of Advanced Manufacturing Technology, 133 (11-12) (2024) 5197-5209. https://doi.org/10.1007/s00170-024-13982-1

[20] I. Kacar, S. Yildirim, Parameter calibration of a novel combined hardening model for a wire drawing simulation of AA7075-T6, Journal of Materials Engineering and Performance, 34 (2025) 8691-8706. https://doi.org/10.1007/s11665-024-10377-x

[21] A. Whelan, T. Tang, V. Pakrashi, P. Cardiff, A finite volume framework for damage and fracture prediction in wire drawing, International Journal for Numerical Methods in Engineering, 126 (1) (2025) 1-42. https://doi.org/10.1002/nme.7640

[22] F.J. Doblas-Charneco, D. Morales-Palma, A. Estévez, C. Vallellano, Mathematical optimization of cold wire drawing operations, Advances in Science and Technology, 132 (2023) 13-21. https://doi.org/10.4028/p-3lhBRy

[23] T.G. dos Santos, A. Rosiak, D.R. Alba, D.P. Wermuth, M.H. Riffel, R.P. da Rocha, L. Schaeffer, Experimental-numerical analysis to determine the efficiency of industrial lubricants in wire drawing process, Revista de Metalurgia, 59 (1) (2023) 1-10. https://doi.org/10.3989/revmetalm.234

[24] E. Ruiz, M. Cuartas, D. Ferreno, L. Romero, V. Arroyo, F. Gutierrez-Solana, Optimization of the fabrication of cold drawn steel wire through classification and clustering machine learning algorithms, IEEE Access, 7 (2019) 141689-141700. https://doi.org/10.1109/ACCESS.2019.2942957

[25] R.J. Kuo, Z.X. Xu, Predictive maintenance for wire drawing machine using MiniRocket and GA-based ensemble method, The International Journal of Advanced Manufacturing Technology, 134 (3-4) (2024) 1661-1676. https://doi.org/10.1007/s00170-024-14225-z

[26] P. Kumar, G. Agnihotri, Cold drawing process - a review, International Journal of Engineering Research and Applications, 3 (3) (2013) 988-994.

[27] L.V. Radionova, D.V. Gromov, R.A. Lisovskiy, I.N. Erdakov, Experimental determination and calculation of the wire drawing force in monolithic dies on straight-line drawing machines, Machines, 11 (2) (2023) 1-13. https://doi.org/10.3390/machines11020252

[28] L. Sadok, M. Paćko, A. Skolyszewski, M. Ruminski, Influence of the shape of the die on the field of strains in the drawing process, Journal of Materials Processing Technology, 34 (1-4) (1992) 381-388. https://doi.org/10.1016/0924-0136(92)90131-B

[29] P. Gawali, A.K. Kundu, N. Gautam, Variation in mechanical properties of wire due to variation of speed in wire drawing process, Journal of Emerging Technologies and Innovative Research, 9 (12) (2022) 5-11.

[30] L.V. Radionova, R.A. Lisovskiy, A.S. Svistun, D.V. Gromov, I.N. Erdakov, FEM simulation analysis of wire drawing process at different angles dies on straight-line drawing machines, Proceedings of the 8th International Conference on Industrial Engineering, Sochi, Russia, 2022, pp. 769-778.

[31] S.Y. Lee, I.K. Lee, S.K. Lee, S.K. Hwang, D. Park, Fabrication of 30.0 μm fine rhodium wire from 80.0 μm initial wire using multi-pass wire drawing process, Journal of Mechanical Science and Technology, 35 (6) (2021) 2637-2644. https://doi.org/10.1007/s12206-021-0534-z

[32] S. Verma, P.S. Rao, Multistage wire drawing process analysis and optimization of process parameters, International Journal of Technical Innovation in Modern Engineering & Science, 5 (1) (2019) 173-183.

[33] S. Wiewiórowska, Z. Muskalski, The influence of the partial single reduction on mechanical properties wires made from TRIP steel with 0.43% C, Metalurgija, 54 (1) (2015) 184-186.

[34] S.M. Lee, I.K. Lee, S.Y. Lee, M.S. Jeong, Y.H. Moon, S.K. Lee, Evaluation of radial direction non-uniform strain in drawn bar, Transactions of Materials Processing, 29 (6) (2020) 356-361. https://doi.org/10.5228/KSTP.2020.29.6.356

[35] Á. González, M. Cruchaga, D. Celentano, J.P. Ponthot, Damage prediction in the wire drawing process, Metals, 14 (10) (2024) 1-16. https://doi.org/10.3390/met14101174

[36] M. Suliga, P. Szota, M. Gwoździk, J. Kulasa, A. Brudny, The influence of temperature in the wire drawing process on the wear of drawing dies, Materials, 17 (20) (2024) 1-23. https://doi.org/10.3390/ma17204949

[37] S. Wiewiórowska, Analysis of the influence of drawing process parameters on the mechanical properties of TRIP-structure steel wires, Archives of Metallurgy and Materials, 58 (2) (2013) 573-578. https://doi.org/10.2478/amm-2013-0040

[38] P. Skubisz, M. Rumiński, Ł. Lisiecki, Estimation of strain-hardness correlation in cold-forged austenitic stainless steel, Key Engineering Materials, 622-623 (2014) 179-185. https://doi.org/10.4028/www.scientific.net/KEM.622-623.179

[39] J. Toribio, M. Lorenzo, Influence of the straining path during cold drawing on the hydrogen embrittlement of prestressing steel wires, Metals, 13 (7) (2023) 1-14. https://doi.org/10.3390/met13071321

[40] W. He, F. Li, H. Zhang, H. Chen, H. Guo, The influence of cold rolling deformation on tensile properties and microstructures of Mn18Cr18 N austenitic stainless steel, Materials Science and Engineering A, 764 (2019) 138245. https://doi.org/10.1016/j.msea.2019.138245

[41] H. Tschaetsch, Metal forming practise, Springer-Verlag, Berlin Heidelberg, 2006, pp. 96-97.

[42] I. Kniazkin, R. Pelaccia, M. Negozio, S. Di Donato , L. Donati, B. Reggiani, N. Biba, R. Rezvykh, I. Kulakov, Investigation of the skin contamination predictability by means of QForm UK extrusion code, Materials Research Proceedings, 28 (2023) 543-552. https://doi.org/10.21741/9781644902479-59

[43] H. Wang, W. Wang, R. Zhai, R. Ma, J. Zhao, Z. Mu, Constitutive equations for describing the warm and hot deformation behavior of 20Cr2Ni4A alloy steel, Metals, 10 (9) (2020) 1-30. https://doi.org/10.3390/met10091169

[44] P. Vo, M. Jahazi, S. Yue, P. Bocher, Flow stress prediction during hot working of near-α titanium alloys, Materials Science and Engineering A, 447 (1-2) (2007) 99-110. https://doi.org/10.1016/j.msea.2006.10.032

[45] M. Rumiński, Stan odkształcenia oraz rozkład własności mechanicznych w ciągnionych rurach

stalowych (State of strain and distribution of mechanical properties in drawn steel tubes), PhD thesis, AGH University of Krakow, 1999.

[46] H. Oktadinata, T. Triantoro, A. Gumilar, U.R. Jatmiko, Microstructure and hardness properties of AISI 321 stainless steel welded joints with different filler metal, Key Engineering Materials, 951 (2023) 3-9. https://doi.org/10.4028/p-GOU7ql

[47] H.U. Rehman, M. Naeem, M. Abrar, M. Shafiq, J.C. Díaz-Guillén, Muhammad Yasir, Shahid Mahmood, Enhancement of hardness and tribological properties of AISI 321 by cathodic cage plasma nitriding at various pulsed duty cycle, Journal of Alloys and Compounds, 1002 (2024) 175280. https://doi.org/10.1016/j.jallcom.2024.175280

[48] A.A. Tiamiyu, J.A. Szpunar, A.G. Odeshi, Strain rate sensitivity and activation volume of AISI 321 stainless steel under dynamic impact loading: Grain size effect, Materials Characterization, 154 (2019) 7-19. https://doi.org/10.1016/j.matchar.2019.05.027

[49] A.A. Tiamiyu, U. Eduok, J.A. Szpunar, A.G. Odeshi, Corrosion behavior of metastable AISI 321 austenitic stainless steel: Investigating the effect of grain size and prior plastic deformation on its degradation pattern in saline media, Scientific Reports, 9 (1) (2019) 1-18. https://doi.org/10.1038/s41598-019-48594-3

[50] K.I. Emurlaev, I.A. Bataev, D.V. Lazurenko, V.G. Burov, I.V. Ivanov, Y.Y. Emurlaeva, Deformation-induced martensite transformation in AISI 321 stainless steel under dry sliding friction, Materials Today: Proceedings, 25 (2020) 424-427. https://doi.org/10.1016/j.matpr.2019.12.140

UTICAJ STEPENA REDUKCIJE NA POPUNJENOST KALUPA I PROFIL TVRDOĆE KOD HLADNO VUČENIH POLIGONALNIH ŠIPKI OD NERĐAJUĆEG ČELIKA OTPORNOG NA KISELINE X6CrNiTi18-10

M. Rumiński [a], P. Skubisz [a,*], P. Micek [b]

[a] AGH Univerzitet u Krakovu, Fakultet za inženjerstvo metala i industrijsku računarsku nauku, Krakov, Poljska

[b] AGH Univerzitet u Krakovu, Fakultet za mašinstvo i robotiku, Krakov, Poljska

Apstrakt

Ova studija istražuje uticaj stepena redukcije na efikasnost deformacionog ojačavanja i opterećenje tokom procesa vučenja austenitnog nerđajućeg čelika otpornog na kiseline X6CrNiTi18-10. Fokus je na optimizaciji geometrijski povezanih procesnih uslova radi postizanja najvišeg kvaliteta i produktivnosti pri vučenju šipki specijalne namene poligonalnog oblika, konkretno kvadratnog i heksagonalnog preseka. Istraživanje se bavi time kako povećanje stepena redukcije može poboljšati deformaciono ojačavanje uz istovremeno smanjenje broja operacija vučenja, što na kraju utiče na kvalitet i opterećenje. Numeričko modelovanje je korišćeno za analizu odnosa između deformacionog ojačavanja i opterećenja u funkciji stepena redukcije. Odgovarajući modeli i pretpostavke su formulisani, a zatim verifikovani eksperimentima, koji su potvrdili valjanost matematičkih i numeričkih modela za procenu opterećenja. Studija je kvantifikovala efekat deformacije na čvrstoću merenjem profila tvrdoće duž gradijenta deformacije. Primena gredica promenljivih prečnika proizvela je slične profile tvrdoće za obe analizirane geometrije šipki i obrnula efekat nedovoljne popunjenosti uglova matrice. Rezultati ukazuju na granični stepen redukcije za izradu ispravnih šipki kvadratnog ili heksagonalnog preseka. Prekoračenje te granice može izazvati prekomerno deformaciono ojačavanje, što rezultira povećanom tvrdoćom koja otežava popunjenost uglova i/ili dovodi do loma.

Ključne reči: *Hladno vučenje; Čelik otporan na kiseline; Čelik X6CrNiTi18-10; Deformaciono ojačavanje; Modelovanje metodom konačnih elemenata; Tvrdoća*